Scripta Materialia 133 (2017) 1–4

Contents lists available at ScienceDirect

Scripta Materialia

journal homepage: www.elsevier.com/locate/scriptamat

Regular Article

Intrinsic fracture toughness of bulk nanostructured Cu with nanoscale deformation twins

S.S. Luo [a], Z.S. You [a,b], L. Lu [a,*,1]

[a] Shenyang National Laboratory for Materials Science, Institute of Metal Research, Chinese Academy of Sciences, 72 Wenhua Road, Shenyang 110016, People's Republic of China
[b] Herbert Gleiter Institute of Nanoscience, Nanjing University of Science and Technology, 200 Xiaolingwei Street, Nanjing 210094, People's Republic of China

ARTICLE INFO

Article history:
Received 21 November 2016
Received in revised form 17 January 2017
Accepted 28 January 2017
Available online 7 February 2017

Keywords:
Fracture toughness
Nanostructured metals
Digital image correlation
Nanotwins
Crack tunneling

ABSTRACT

A contactless video crack opening displacement gauging system based on digital image correlation technique was established to measure the load-line displacement of miniaturized fracture toughness samples precisely. The intrinsic fracture toughness and smoothly rising *R*-curve of bulk dynamic plastic deformation (DPD) Cu with nanotwin bundles embedded in nano-grained matrix were measured through elastic-plastic unloading compliance method using miniaturized side-grooved compact tension specimens. Nanotwin bundles exert positive bearings on enhancing the damage tolerance of the DPD Cu.

Refining grains to the nanometer scale provides attractive mechanical properties such as high strength/hardness and superior wear resistance [1,2], but it is generally conjectured that the high strength is inevitably accompanied by reduced ductility and poor damage tolerance [3–5]. This disadvantage would strongly limit the potential engineering applications of the nanostructured materials. In contrary to extensive studies on the ductility [6–8], reliable quantitative fracture mechanics evaluation of nanostructured materials is still rather limited so far [9–13]. This scarcity stems mainly from the fact that current existing techniques for preparing nanostructured materials cannot deliver sufficient specimen volume required for conventional fracture tests, thus the geometry-independent intrinsic fracture toughness is generally unavailable.

In order to evaluate the intrinsic fracture properties of nanostructured materials, the elastic-plastic fracture mechanics (EPFM) methods, which take account of crack tip plasticity, are usually applied for samples with miniaturized geometries [9,13,14]. Previous investigations have attempted to measure the elastic-plastic *J*-integral fracture toughness of bulk ultrafine-grained (UFG) metals prepared by severe plastic deformation [10–12]. The prerequisite of *J*-integral measurement is that the load-line displacement (LLD) must be precisely measured in order to compute the energy input to the tested sample. Conventionally, the LLD of standard fracture toughness specimen is easily determined by using an electron-mechanical clip-on COD gauge. However, such COD gauges are not applicable for the miniaturized nanostructured samples caused by their limited crack mouth spaces. How to accurately measure the LLD of miniaturized nanostructured materials becomes an unsolved challenge.

Dynamic plastic deformation (DPD) is an effective technique to prepare a novel bulk nanostructured Cu consisting of nano-grained matrix and embedded bundles of nanoscale deformation twins. The influence of the nanotwinned structure on the fracture behavior of the DPD Cu had been investigated in terms of single-edge notched bending tests by using miniaturized specimens [15,16]. The introduction of nanotwin bundles was found to increase the fracture toughness by promoting the formation of coarse/deep dimples [15,16]. However, because the linear elastic condition or the small-scale yielding condition was not satisfied, the intrinsic fracture toughness might be largely underrated.

In this study, the intrinsic fracture behavior of the DPD Cu is carefully evaluated by EPFM using a custom-designed contactless COD gauge with a high accuracy. Both the critical *J*-integral fracture toughness and crack growth resistance behavior are analyzed.

To accurately measure the LLD of miniaturized specimens, a contactless video crack opening displacement (VCOD) gauging system was developed based on digital image correlation (DIC) technique. The major components of the VCOD gauging include a Moritex telecentric optical lens, a high resolution CMOS camera and a computer with a custom-designed software for automatically capturing and analyzing images (Fig. 1a). The lens has a fixed magnification of 2× and a working distance of 65 mm. The resolution of the camera is 2592 × 1944 pixels, with a physical pixel size of 2.2 μm. Miniaturized

* Corresponding author.
E-mail address: llu@imr.ac.cn (L. Lu).
[1] Prof. Lei Lu was an editor of the journal during the review period of the article. To avoid a conflict of interest, Prof. Irene J. Beyerlein acted as editor for this manuscript.

http://dx.doi.org/10.1016/j.scriptamat.2017.01.032
1359-6462/

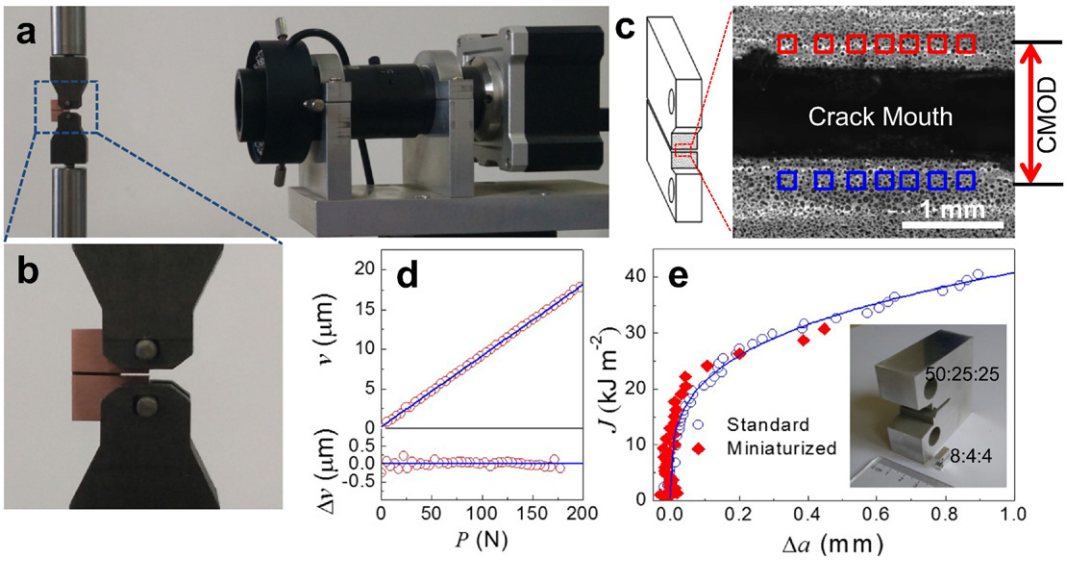

Fig. 1. (a) The VCOD gauging system based on digital image correlation (DIC) technique. (b) The compact tension (CT) specimen in (a). (c) Random speckle patterns at both sides of the CT specimen used for obtaining the load-line displacement (LLD). (d) The LLD versus force diagram measured by the VCOD. (e) The *J*-integral resistance (*J*-*R*) curves for miniaturized and standard specimens (inset image) tested by the VCOD and commercial clip-on COD gauge, respectively.

compact tension (CT) fracture toughness specimen with a width W of ~8.0 mm and a thickness B of ~4.0 mm was used, as shown in Fig. 1b. To mimic the measuring of conventional COD gauge, a random speckle pattern was firstly prepared by spraying black ink onto white paint background at the load plane, namely the common plane of the two pin hole centers (Fig. 1c). The original image before testing was captured as a reference image and several subsets (21 × 21 pixels) above and below the crack mouth were manually selected as tracing markers (Fig. 1c). Real-time images continuously captured by the digital camera during testing were automatically analyzed by the computer program to obtain relative displacements of the selected subsets with respect to the reference image. Since the pattern coincides with the load plane, the relative displacement representing the instantaneous crack mouth opening displacement (CMOD) can be regarded as the LLD without geometrical modification.

Fig. 1d shows a good linear relationship between the measured LLD and the imposed force during the elastic loading stage of a CT specimen. The slope representing the compliance of the specimen is 0.447 μm/N, which is quite close to the theoretical value (0.439 μm/N) calculated by the compliance equation of the CT specimen [14]. The LLD-force relationship not only demonstrates the accuracy (with a maximum deviation ≤0.3 μm) of the LLD measurement, but also proves that the measured compliance is sufficiently accurate to calculate the instantaneous crack length, which is also essential for EPFM evaluation. Therefore, the conventional single specimen technique can be employed with the stable crack advance being determined through measuring the instantaneous compliance by partially unloading the sample. Additionally, it has also been demonstrated that the contactless VCOD is sufficiently accurate to monitor crack extension of brittle materials which exhibit only limited crack tip opening displacement prior to complete fracture.

In order to verify the accuracy of the VCOD and the reliability of determining the intrinsic fracture resistance curve using a miniaturized specimen, comparison tests are performed on a commercial 7075-T651 aluminum alloy (with an average grain size of 24 ± 3 μm and a yield strength of 451 ± 4 MPa). Miniaturized specimens with a side-groove of 10%B (required for obtained plane-strain toughness, as discussed below) based on the VCOD and standard specimens (W = ~50.0 mm, B = ~25.0 mm, a_0 = ~25 mm, non-side-grooved) with a commercial clip-on COD gauge, as shown in the inset of Fig. 1e, were tested following the procedure in accordance with ASTM E1820 [14]. In spite of the large difference in the specimen geometries, coincident curves of *J*-integral in Fig. 1e as a function of crack extension can be obtained. The comparison tests verify that the fracture toughness measured by miniaturized specimens is valid and the results are comparable to the conventional approaches.

Based on the contactless VCOD gauging system, the fracture behavior of the DPD Cu was investigated using the single specimen technique following the standard procedure of ASTM E1820 [14]. In order to obtain a sharp initial crack front, the CT specimens were first notched to a depth of ~3.2 mm by electrical discharge machining, and then fatigue pre-cracked in a tension-tension mode at a frequency of 2 Hz until an initial total crack length a_0 of ~4.0 mm was reached. The crack plane normal is in the tangential direction of the DPD Cu disk while the expected direction of crack propagation is coincident with the radial direction. The specimens were loaded under displacement control at a speed of about 0.1 mm/min to stimulate crack extension. With the recorded force, LLD measured by the VCOD and instantaneous compliance, the *J*-integral as a function of crack extension can be determined by the standard procedure in ASTM E1820 [14].

Fig. 2 shows the transverse microstructure of the DPD Cu with a total accumulated true strain of 2.0. The true strain $\varepsilon = \ln(h_i/h_f)$, where h_i and h_f are the initial and final sample thicknesses, respectively. A mixed microstructure with bundles of nanoscale deformation twins (region A) embedded in a matrix of nano-grains (region B) was obtained. Statistics show that the volume fraction of the nanotwin bundles is ~35%, and the average twin thickness is 47 ± 3 nm (Fig. 2b). Fig. 2c displays that the nano-grains are slightly elongated with a mean transverse size of 69 ± 4 nm. Uniaxial tensile tests at room temperature show that the 0.2% offset yield strength (σ_{ys}) and the ultimate tensile strength (σ_{uts}) of the DPD Cu are 595 ± 8 MPa and 629 ± 11 MPa, respectively, while the elongation to failure (δ_f) is 5.9 ± 0.5%, consistent with Ref. [16].

The representative force versus LLD curve of DPD Cu is shown in Fig. 3a. After reaching the peak value, the force decreases steadily with increasing LLD, a consequence of stable crack growth. The computed *J*-integral as a function of crack extension Δa, namely the *J*-integral resistance (*J*-*R*) curve, is displayed in Fig. 3b. The *J*-integral monotonically increases as crack advancing, apparently manifesting a rising *J*-*R* curve behavior, which is in agreement with the measurements of other miniaturized nanostructured specimens [9,13]. However, the overview micrograph (Fig. 3e) of the final crack front delineated by

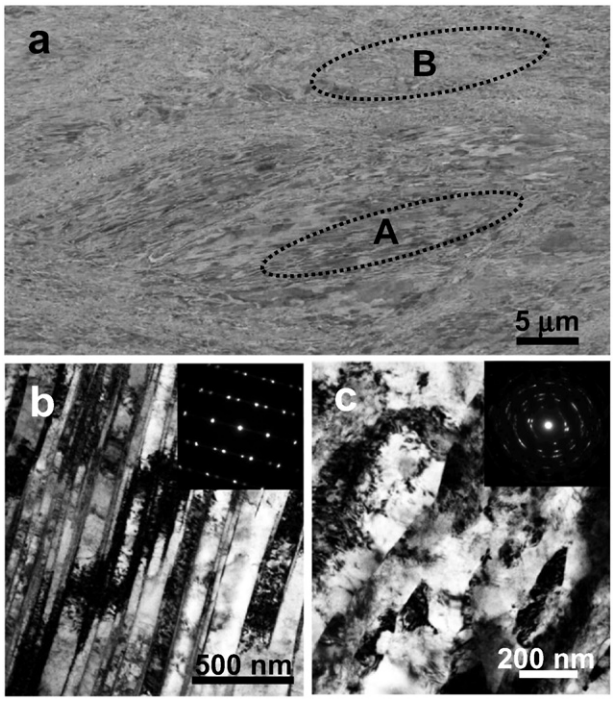

Fig. 2. (a) SEM observation on the transverse microstructure of the DPD Cu, in which nanotwin bundles embedded in nano-grained matrix. (b) and (c) TEM observations on the nanotwin bundles (region A) and nano-grained matrix (region B), respectively.

post-fatigue demonstrates that the crack front is rather curved with a long propagation distance in the specimen center, and a negligible propagation distance on the specimen surfaces. Due to the presence of such crack tunneling, the trailing segments drag the broken surfaces, leading to the observed growing crack extension resistance. The extra toughening extrinsically caused by the crack tunneling would be more significant as specimen size reduces. Therefore, the observed *J*-*R* curve behavior cannot reflect the inherent fracture property of the DPD Cu.

In order to eliminate the crack tunneling, side-grooving was generally applied to enhance the stress triaxiality at the sample surfaces [17–19]. For this purpose, two grooves with a depth of ~0.4 mm and a root radius of ~50 μm were cut along the crack propagation plane on both specimen sides. To guarantee the crack front straightness, the fatigue pre-cracking had been performed prior to the side grooving. Then the side-grooved specimens with a net thickness (B_N) of ~3.2 mm were tested under the same displacement control condition. Compared with Fig. 3a, the force decreases more precipitously with increasing LLD after the peak force (Fig. 3c), manifesting that the crack extends more easily with side-grooves. The calculated *J*-*R* curve shows a reduced increasing rate of the *J*-integral with Δa compared with the non-side-grooved case (Fig. 3d).

Overall fracture surface observations in Fig. 3f reveal that the crack tunneling has been effectively suppressed: the crack front is held straight during crack extension and the crack propagates uniformly. As required by the ASTM standard [14], the difference of each crack size should be less than 0.05*B*, measured at nine equally spaced points along the initial and final crack front. Obviously, the substantial crack tunneling in the non-side-grooved specimen violates this requirement. For the side-grooved specimen, the largest deviations from the corresponding average crack lengths are 0.10 mm and 0.13 mm for the initial fatigue pre-crack and the final stable crack, respectively. Both values are less than 0.05*B*, indicating that the straight crack front requirement is satisfied by side-grooving, thus a valid *J*-*R* curve of the DPD Cu can be obtained.

Based on the accurately determined *J*-*R* curve, a provisional critical *J*-integral value, J_Q, is generally defined as the intersection of the *J*-*R* curve with the 0.2 mm offset blunting line, $J = 2\sigma_Y \Delta a$, where $\sigma_Y = (\sigma_{ys} + \sigma_{uts})/2$. Since the *J*-*R* curve determined using miniaturized specimens coincides with that measured using standard specimens, the 0.2 mm offset convention can still be employed. This yields a J_Q of 24 ± 2 kJ m^{-2}. Furthermore, considering both the thickness *B* and the initial crack ligament b_0 ($= W - a_0$) are larger than $25J_Q/\sigma_Y$ (0.99 mm), J_Q can be qualified as the intrinsic size-independent fracture toughness J_{IC}. This point is further experimentally verified by measuring the critical *J*-integral as a function of sample thickness. It evidently shows that $B = 4$ mm has exceeded the critical thickness above which the *J*-integral becomes relatively constant and the obtained J_{IC} thus represents the intrinsic plane strain fracture resistance of the DPD Cu. The corresponding critical stress intensity factor, K_{JC}, can be calculated from the following relationship:

$$K_{JC} = \sqrt{\frac{EJ_{IC}}{1-\nu^2}} \tag{1}$$

where the Young's modulus $E = 120$ GPa, and the Poisson ratio $\nu = 0.3$. Thus, the K_{JC} of DPD Cu is 56 ± 3 MPa m$^{1/2}$.

Alternatively, the fracture initiation toughness can also be estimated by measuring the critical stretch zone width (SZW_C) in the mid-section

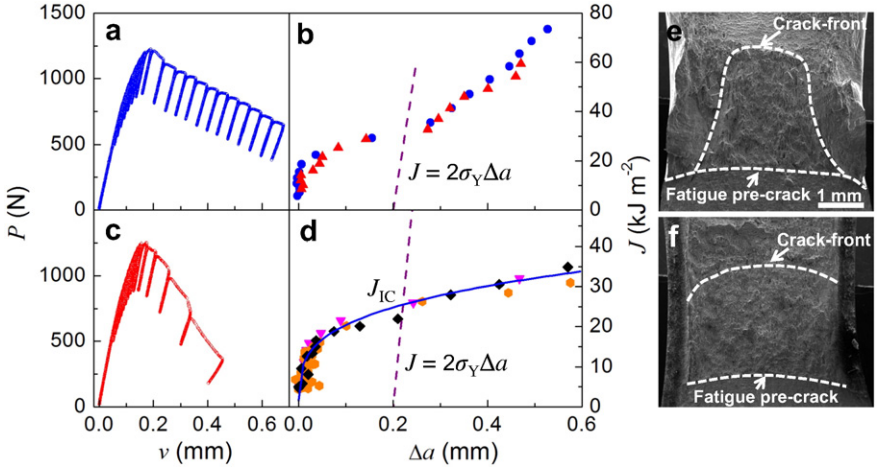

Fig. 3. (a) and (c) The force versus LLD curves for the plane and side-grooved miniaturized CT specimens of the DPD Cu. (b) and (d) Computed *J*-integral resistance (*J*-*R*) curves for the two specimens from the data in (a) and (c). (e) and (f) The macroscopic fracture surfaces for the plane and side-grooved specimens, indicate that the crack tunneling could be eliminated effectively by the side-grooving design.

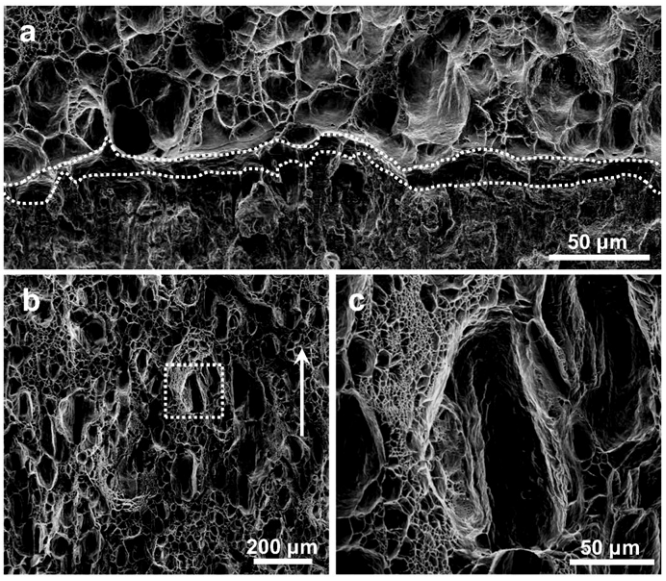

Fig. 4. (a) The stretch zone of the DPD Cu is surrounded inside the dash lines. (b) SEM observation on the fracture surface of the DPD Cu under plane strain condition, the white arrow indicates the main crack growth orientation. (c) The magnification of the coarse/deep dimples in (b), specially, the fine/shallow dimples are mainly aggregated surrounding the coarse/deep dimples.

of fractured samples under plane strain condition. The stretch zone is defined as the transition area between the fatigue pre-crack tip and the stable crack growth zone [20], as shown in Fig. 4a, which reflects the magnitude of crack tip blunting before the onset of stable crack extension. The critical *J*-integral, J_{SZW}, of fracture initiation is estimated from the average SZW_C (9 ± 1 μm) by the following relationship [10,20]:

$$J_{SZW} = 4\sigma_Y SZW_C \quad (2)$$

This yields $J_{SZW} = 23 \pm 2$ kJ m^{-2}, in consistent with that measured by means of the *J-R* curve, a further certification that the nanostructured DPD Cu possesses a considerable inherent fracture toughness in conjunction with a high flow stress, which is probably associated with the existing nanotwin bundles.

Fig. 4b illustrates the fractograph in the middle section of a side-grooved sample after fracture toughness test. In consistent with the fractographic observations on three-point bending specimens [15,16], the fracture surface consists of three typical types of heterogeneously distributed dimples: coarse/deep dimples, equiaxed middle dimples and fine/shallow dimples. The small ductile dimples are usually detected on the fracture surface of nano-grained materials [21,22]. In contrary to general coarse-grained metals, the coarse/deep dimples (Fig. 4c) are confirmed to be irrelevant to non-metallic inclusions. Instead, the deformation twin bundles play an essential role in producing such coarse dimples which dissipate large irreversible plastic energy and increase crack growth resistance [16].

The toughening effect of nanotwinned structures have been investigated by several recent experimental studies and molecular dynamics simulations [13,23–29]. It is recognized that the low energy coherent twin boundaries (TBs) are more resistant to direct micro-void nucleation than incoherent nanoscale grain boundaries (GBs) [13]. This is ascribed to the fact that diverse interactions between dislocations and TBs effectively mitigate the stress concentration or strain incompatibility along TBs [27]. Furthermore, once a crack/void eventually nucleates, in-situ TEM observations demonstrate that its extension can be impeded by such processes as crack tip blunting through dislocation emission along TBs [29], periodical crack deflection in twin/matrix lamellae [23], and crack bridging by twin lamellae [25]. These observations point to a promising strategy to enhance the damage tolerance of nanostructured metals by engineering the internal nanoscale interfaces to include more coherent TBs as illustrated in this study or other special GBs with strong cohesion and resistance to void nucleation.

The incorporation of nanoscale twin bundles as appealing strengthening and toughening agents is highly practical in pure metals [15,16] and alloys, like 316 L stainless steel [9,13]. Considering the complexity of nanotwinned structures, microstructural parameters such as volume fraction, spatial distribution, and length scale of these nanotwin bundles might exert profound influences on the overall toughening behavior. Given the above analysis, understanding on the essential roles that the nanotwin bundles play to mediate the main crack extension and its toughening mechanisms is of significant importance and worthy of in-depth study both in theories and engineering applications.

In summary, a contactless VCOD gauging system based on digital image correlation technique has been designed, which accurately measures the LLD and enables the EPFM evaluation of bulk nanostructured DPD Cu. Using miniaturized side-grooved CT fracture specimens, this method exactly determines the inherent plane-strain fracture toughness that is independent on specimen size. The presence of nanoscale deformation twins plays positive roles in enhancing the damage tolerance of the nano-grained matrix, shedding lights on a new approach for designing metallic materials with high comprehensive performance.

Acknowledgement

The authors acknowledge financial support from the National Natural Science Foundation of China (Grant Nos. 51420105001, 51371171, 51471172 and 51401211) and the Key Research Program of Frontier Sciences, Chinese Academy of Sciences. Z.Y. acknowledges financial support by Natural Science Foundation of Jiangsu Province, China (Grant No. BK20161498).

References

[1] K.S. Kumar, S. Suresh, M.F. Chisholm, J.A. Horton, P. Wang, Acta Mater. 51 (2003) 387–405.
[2] M.A. Meyers, A. Mishra, D.J. Benson, Prog. Mater. Sci. 51 (2006) 427–556.
[3] R.O. Ritchie, Nat. Mater. 10 (2011) 817–822.
[4] A.A. Karimpoor, K.T. Aust, U. Erb, Scr. Mater. 56 (2007) 201–204.
[5] R.A. Mirshams, C.H. Xiao, S.H. Whang, W.M. Yin, Mater. Sci. Eng. A 315 (2001) 21–27.
[6] Y. Wang, M. Chen, F. Zhou, E. Ma, Nature 419 (2002) 912–915.
[7] Y.M. Wang, E. Ma, Acta Mater. 52 (2004) 1699–1709.
[8] L. Lu, Y. Shen, X. Chen, L. Qian, K. Lu, Science 304 (2004) 422.
[9] L. Xiong, Z.S. You, L. Lu, Scr. Mater. 119 (2016) 55–59.
[10] A. Hohenwarter, R. Pippan, Scr. Mater. 64 (2011) 982–985.
[11] A. Hohenwarter, R. Pippan, Mater. Sci. Eng. A 540 (2012) 89–96.
[12] A. Hohenwarter, R. Pippan, Acta Mater. 61 (2013) 2973–2983.
[13] L. Xiong, Z.S. You, L. Lu, Scr. Mater. 127 (2017) 173–177.
[14] S. Deville, E. Saiz, R.K. Nalla, A.P. Tomsia, Science 311 (2006) 515.
[15] E.W. Qin, L. Lu, N.R. Tao, K. Lu, Scr. Mater. 60 (2009) 539–542.
[16] E.W. Qin, L. Lu, N.R. Tao, J. Tan, K. Lu, Acta Mater. 57 (2009) 6215–6225.
[17] G. Green, J. Knott, Met. Tech. 2 (1975) 422–427.
[18] P.K. Poulose, Eng. Fract. Mech. 26 (1987) 203–211.
[19] X.P. Zhang, Y.W. Shi, Eng. Fract. Mech. 43 (1992) 863–867.
[20] K.F. Amouzouvi, M.N. Bassim, Mater. Sci. Eng. 55 (1982) 257–262.
[21] H. Li, F. Ebrahimi, Acta Mater. 54 (2006) 2877–2886.
[22] C. Xiao, R.A. Mirshams, S.H. Whang, W.M. Yin, Mater. Sci. Eng. A 301 (2001) 35–43.
[23] Z.W. Shan, L. Lu, A.M. Minor, E.A. Stach, S.X. Mao, JOM 60 (2008) 71–74.
[24] Z. Zeng, X. Li, L. Lu, T. Zhu, Acta Mater. 98 (2015) 313–317.
[25] S.-W. Kim, X. Li, H. Gao, S. Kumar, Acta Mater. 60 (2012) 2959–2972.
[26] A. Singh, L. Tang, M. Dao, L. Lu, S. Suresh, Acta Mater. 59 (2011) 2437–2446.
[27] H. Zhou, S. Qu, Nanotechnology 21 (2010) 035706.
[28] H. Zhou, S. Qu, W. Yang, Model. Simul. Mater. Sci. Eng. 18 (2010) 065002.
[29] L. Liu, J. Wang, S.K. Gong, S.X. Mao, Sci. Rep. 4 (2014) 4397.